Supporting Information

for

Molecular Chemistry in a Zeolite:

Genesis of a Zeolite Y-supported Ruthenium Complex Catalyst

*Isao Ogino and Bruce C. Gates**

Department of Chemical Engineering and Materials Science

University of California, Davis, California 95616

Email: bcgates@ucdavis.edu

EXAFS Data Analysis. Analysis of the EXAFS data was conducted with a difference file technique by use of the software XDAPW2 developed by Vaarkamp et al.[1] Each spectrum that was subjected to analysis was the average of four scans. Each spectrum was processed by fitting a second-order polynomial to the pre-edge region and subtracting this from the entire spectrum. The functional that was minimized and the function used to model the data are given elsewhere.[2] The background was subtracted by using cubic spline routines. Reference backscattering amplitudes and phase shifts were calculated with the software FEFF7[3] from crystallographic data for representing the Ru–O and Ru–C contributions of **I**[4]; a RuAl alloy[5] was used for Ru–Al contribution, and ruthenium metal was used for Ru–Ru contribution.[5] Iterative fitting was done in *R* (distance) space. In the fitting, the coordination number *N* representing each contribution, the sigma-squared value $\Delta\sigma^2$, the interatomic distance *R*, and the inner potential correction ΔE_0 were varied until an optimized fit was obtained at each of four *k*-weightings (k^0, k^1, k^2, and k^3).

Errors were estimated on the basis of the standard equations:

$$\varepsilon^2{}_\nu = \frac{P}{NPTS(P-p)} \sum_i^{NPTS} \left(\frac{\chi_{i,\mathrm{exp}} - \chi_{i\text{-model}}}{\sigma_i}\right)^2 \qquad (1)$$

$$\mathrm{v}ariance = \frac{\int [k^n (FT_{\mathrm{model}}(R) - FT_{\mathrm{exp}}(R))]^2 dR}{\int [k^n FT_{\mathrm{exp}}(R)]^2 dR} \times 100 \qquad (2)$$

where $\varepsilon_\nu{}^2$ is the goodness-of-fit parameter, *P* the total number of free parameters, *p* the number of free parameters, NPTS the actual number of points in the *k*-range used for analysis, and σ_i the measurement uncertainty for each data point, in the averaged spectrum.[2,6] The absolute values of $\varepsilon_\nu{}^2$ often found in EXAFS analysis are approximately

10 and sometimes as much as several hundred, in part because estimation of the error σ_i is difficult, and thus ε_v^2 is not scaled well.[7]

We used the following procedure to discriminate between candidate models to represent the data. We checked whether the best-fit EXAFS parameters with each model were physically reasonable, discarding models with unrealistic EXAFS parameters. We examined fit quality, not just overall fit but also fits of individual contributions determined by using the difference file technique. We considered that one fit model with ε_{v1}^2 is significantly better than another model with ε_{v2}^2 only if the equation (3) is satisfied. The right-hand side of the equation (3) is two times the fluctuation of ε_v^2.[7,8]

$$(\varepsilon_{v1}^{\ 2} - \varepsilon_{v2}^{\ 2})/\varepsilon_{v2}^{\ 2} > 2\sqrt{\frac{2}{P-p}} \qquad (3)$$

Peak deconvolution of IR spectra with Pearson VII model

The Pearson VII model is more general than Lorentzian or Gaussian functions. The Pearson VII distribution is shown below. When q approaches 1, the model resembles a Lorentzian in character and as q approaches infinity, it becomes Gaussian.

$$A_i = \sum_{j=1}^{b} \frac{a_j}{p\left(1 + \frac{(v_i - v_j{}^0)^2(2^{1/q_j} - 1)}{p_j}\right)^{q_j}}$$

A_i: values of absorbance predicted by band models

v_i: ith wavenumber

v_j^0: peak center position of the jth band

b: number of bands

p_j: square of the half width at half-height

q_j: band shape

Figure 1S. ^{1}H NMR spectrum characterizing **I**.

Figure 2S. ^{13}C NMR spectrum characterizing **I**.

Figure 3S. Mass spectra characterizing the outlet gas stream during the treatment of Sample 1 in D_2. The blank data was collected with identical conditions without the sample. In both experiments, the signal intensities were normalized with respect to those for He ($m/z = 4$).

Figure 4S. IR spectra (from bottom to top: $Ru(acac)_3$, zeolite supported $Ru(acac)_3$, **I**, and Sample 1). The arrows indicate the band shifts for $\nu_{as}(CCC)_{ring}$.

Figure 5S. IR spectrum characterizing the silica supported ruthenium complex sample.

Figure 6S. Ru–C_l phase- and amplitude- corrected k^1-weighted FT magnitude and imaginary part of difference spectrum (solid line) and fit (dotted line) representing a Ru–C_l contribution to the EXAFS data characterizing Sample 1 according to model **E**.

Figure 7S. Ru–Ru phase- and amplitude- corrected k^3-weighted FT magnitude and imaginary part of difference spectrum (solid line) and fit (dotted line) representing a Ru–Ru contribution to the EXAFS data characterizing Sample 1 according to model **E**.

Figure 8S. Ru–C_l phase- and amplitude- corrected k^1-weighted FT magnitude and imaginary part of the difference spectrum (solid line) and fit (dotted line) representing Ru–C_l contribution to the EXAFS data characterizing Sample 1 according to model **C**.

Figure 9S. Phase- and amplitude- corrected k^1-weighted FT magnitudes and imaginary parts of the difference spectrum (solid lines) and fits representing each contribution (dotted lines) corresponding to structural parameters reported for model **F**.

Figure 10S. IR spectrum characterizing Sample 1 (solid line) and spectral deconvolution (dashed line, fit; dotted line, component peaks).

Figure 11S. IR spectra of zeolite-supported ruthenium complexes with various loadings of ruthenium: solid line, 3 wt % loading; dashed line, 2 wt % loading; dotted line, 1 wt % loading.

Figure 12S. IR spectrum characterizing zeolite-supported ruthenium complex with 2 wt % loading of ruthenium (solid line) and spectral deconvolution (dashed line, fit; dotted line, component peaks).

Figure 13S. IR spectrum characterizing zeolite-supported ruthenium complex with 3 wt % loading of ruthenium (solid line) and spectral deconvolution (dashed line, fit; dotted line, component peaks).

Figure 1S.

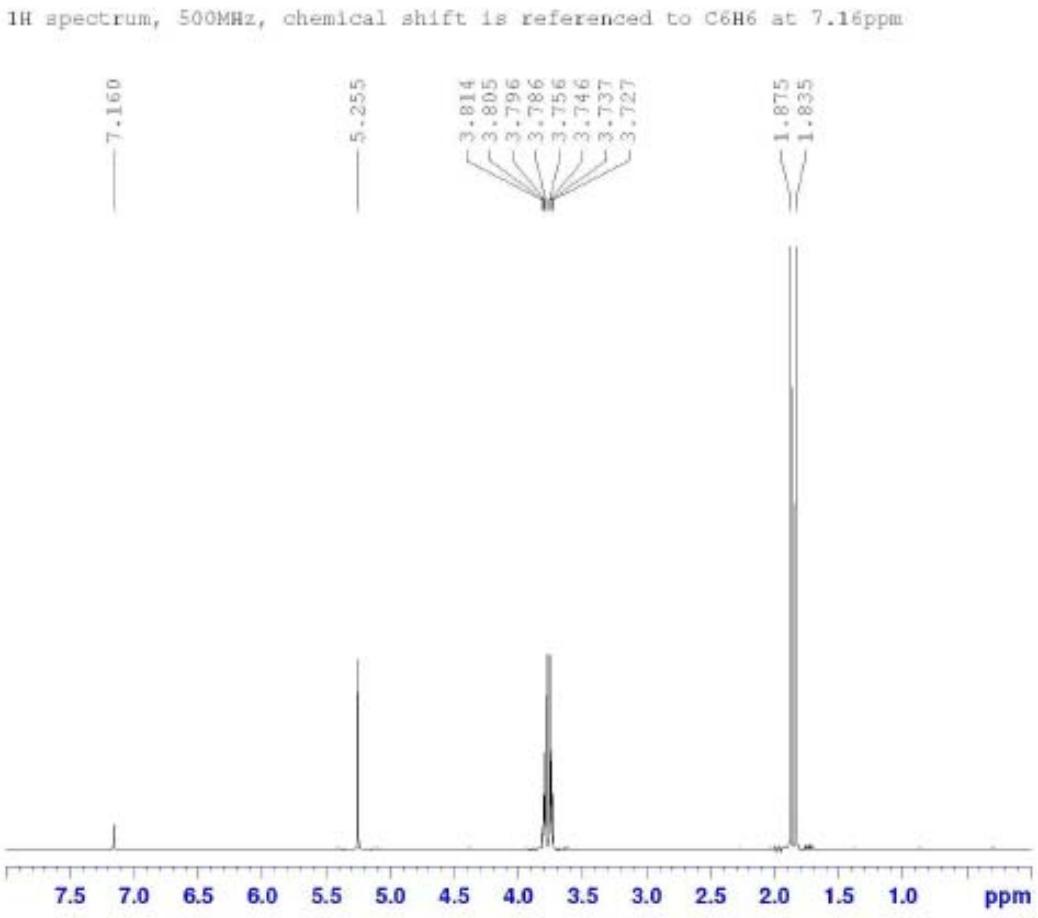
1H spectrum, 500MHz, chemical shift is referenced to C6H6 at 7.16ppm
7.160
5.255
3.814
3.805
3.796
3.786
3.756
3.746
3.737
3.727
1.875
1.835
7.5
7.0
6.5
6.0
5.5
5.0
4.5
4.0
3.5
3.0
2.5
2.0
1.5
1.0
ppm

Figure 2S.

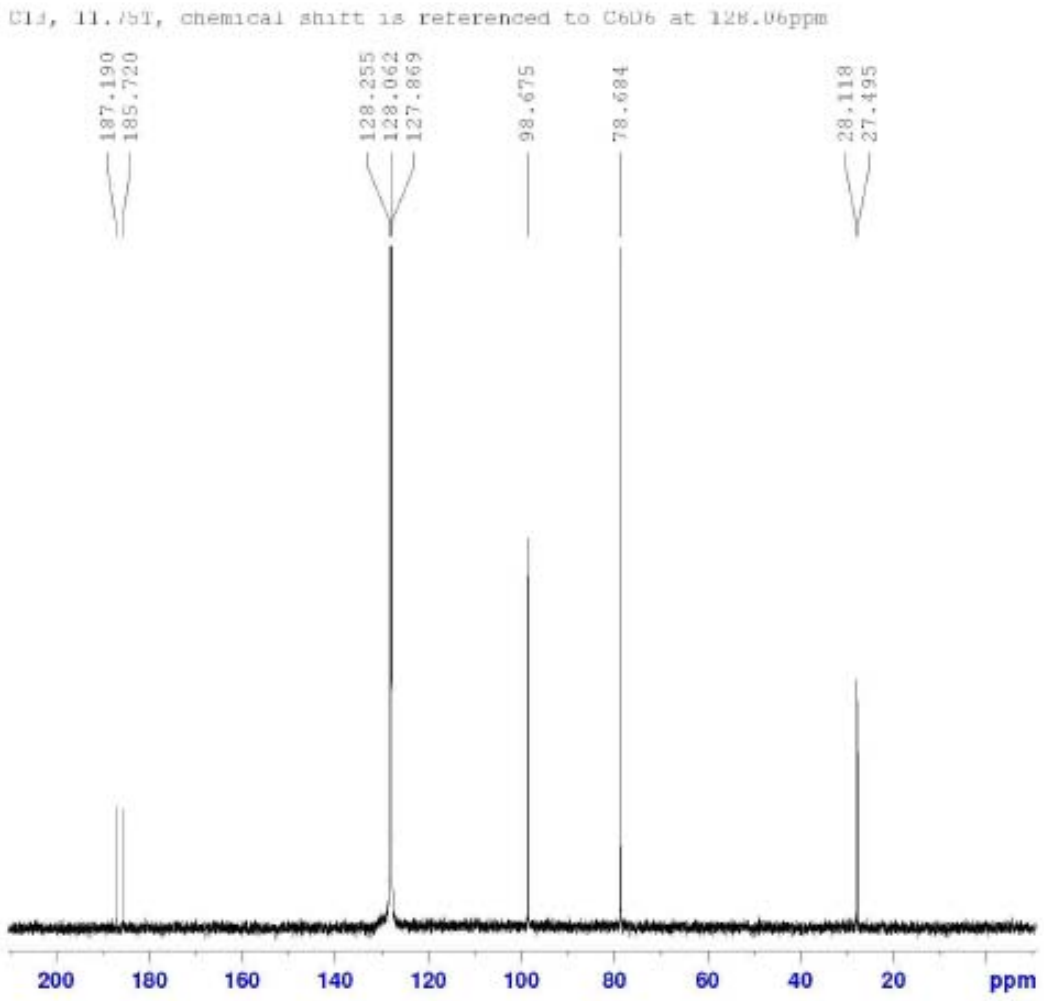
C13, 11.751, chemical shift is referenced to C6D6 at 128.06ppm
187.190
185.720
128.255
128.062
127.869
98.675
78.684
28.118
27.495
200
180
160
140
120
100
80
60
40
20
ppm

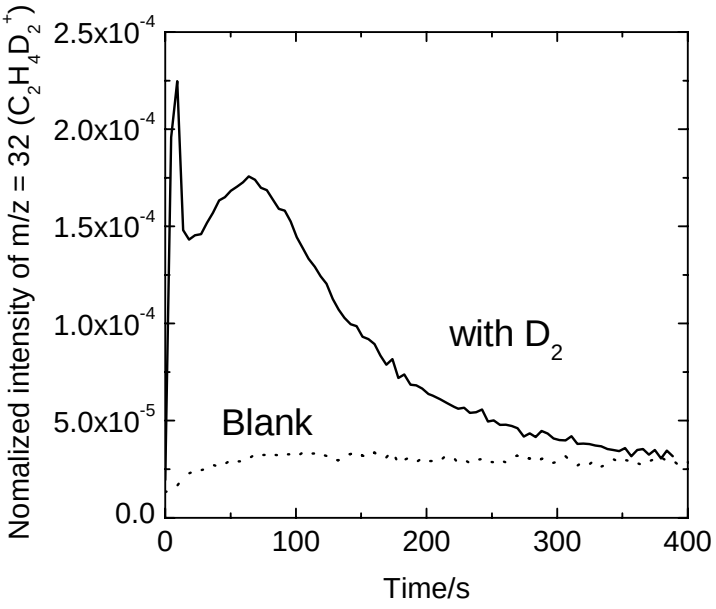

Figure 3S.

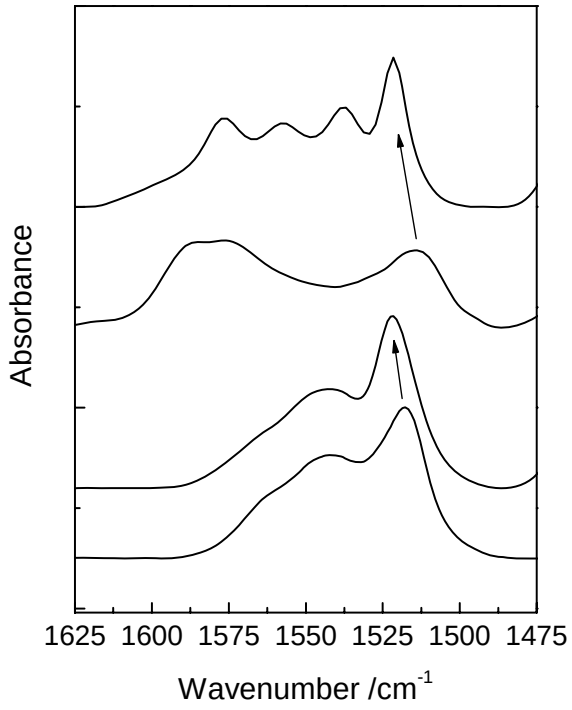

Figure 4S.

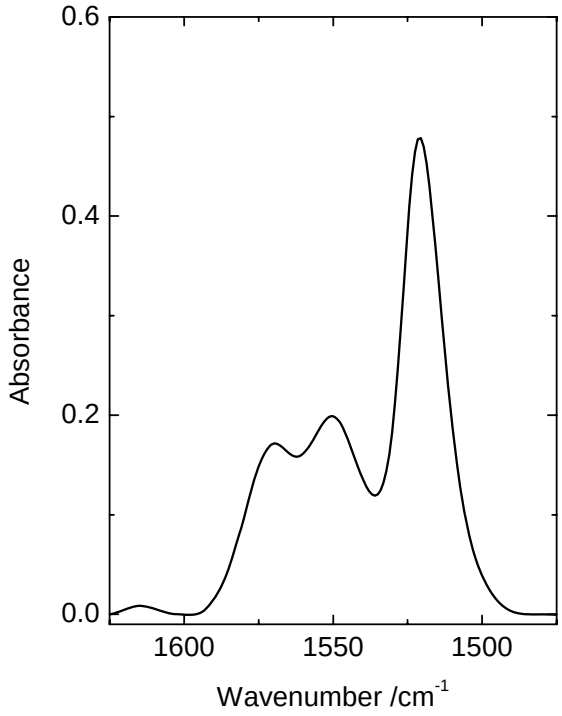

Figure 5S.

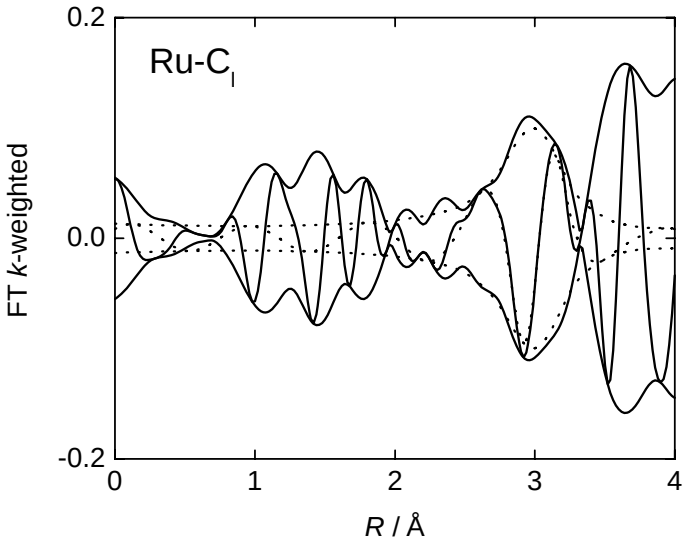

Figure 6S.

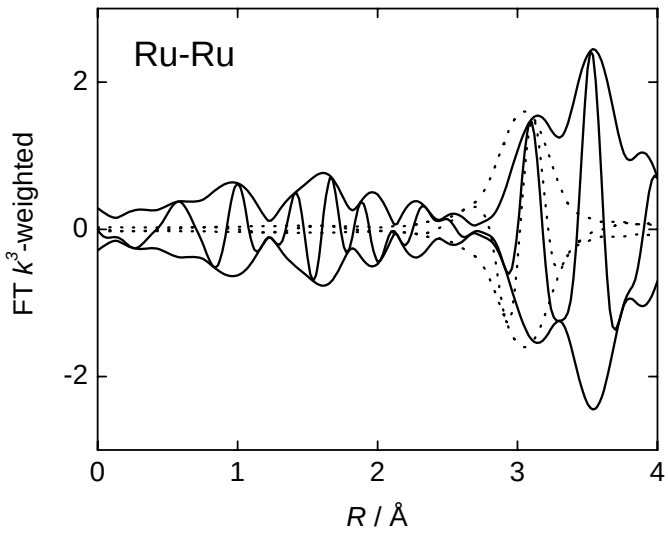

Figure 7S.

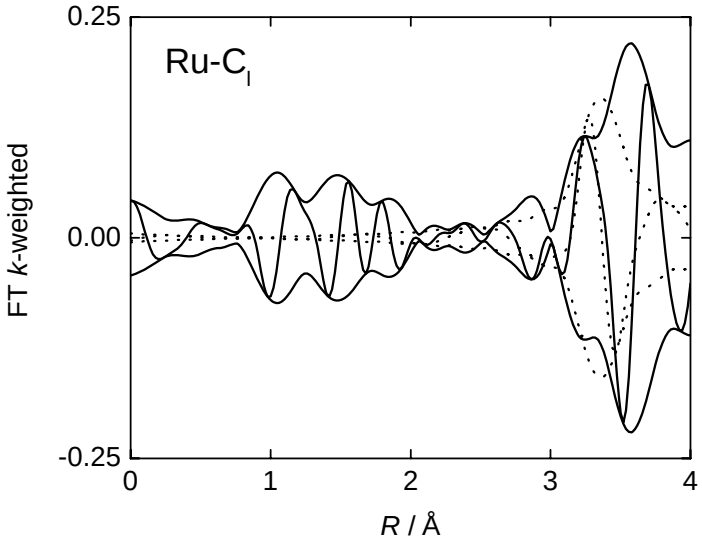

Figure 8S.

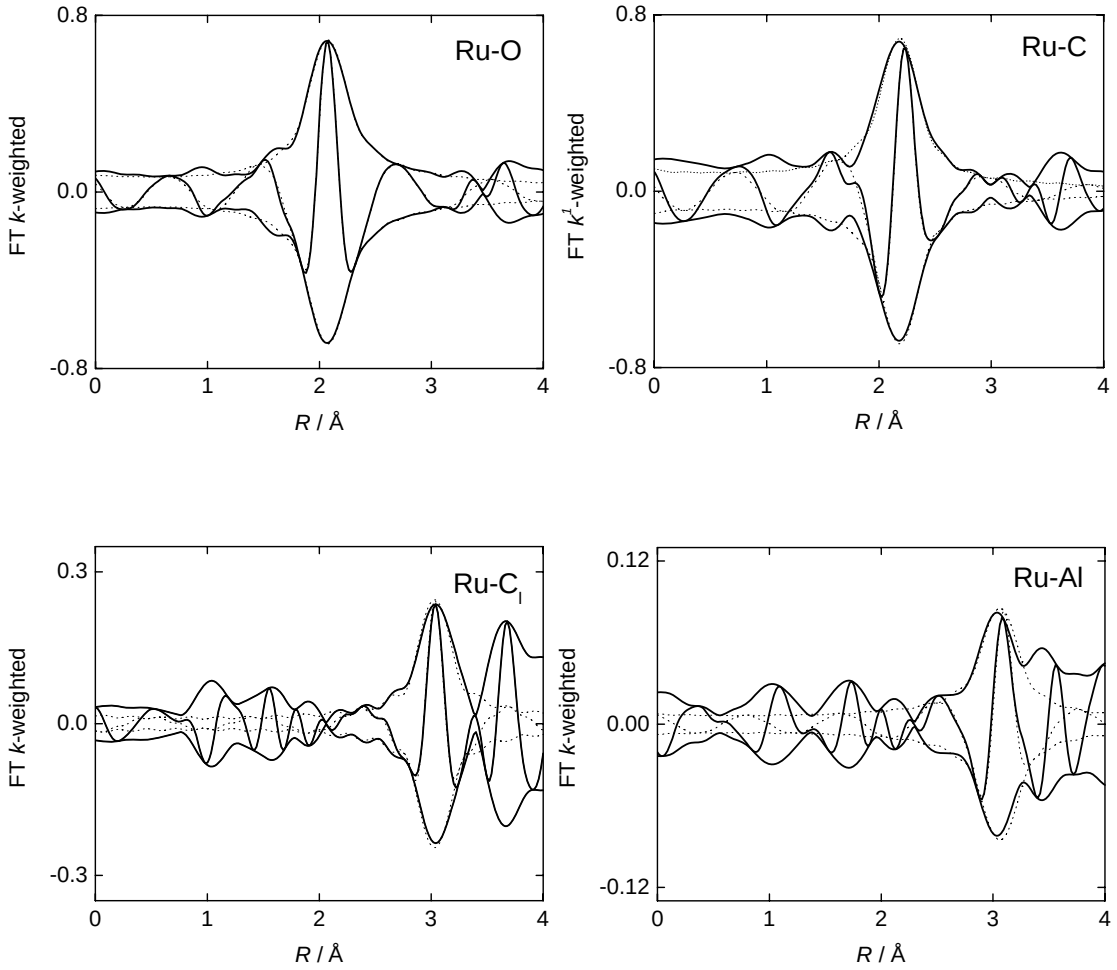
Ru-O
Ru-C
Ru-C$_I$
Ru-Al
FT k-weighted
FT k^1-weighted
R / Å
0.8
0.0
-0.8
0.3
-0.3
0.12
0.00
-0.12
0
1
2
3
4

Figure 9S.

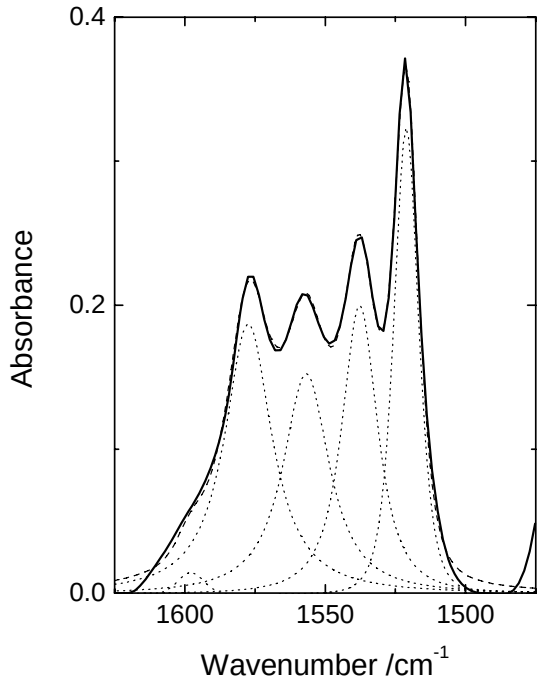

Figure 10S.

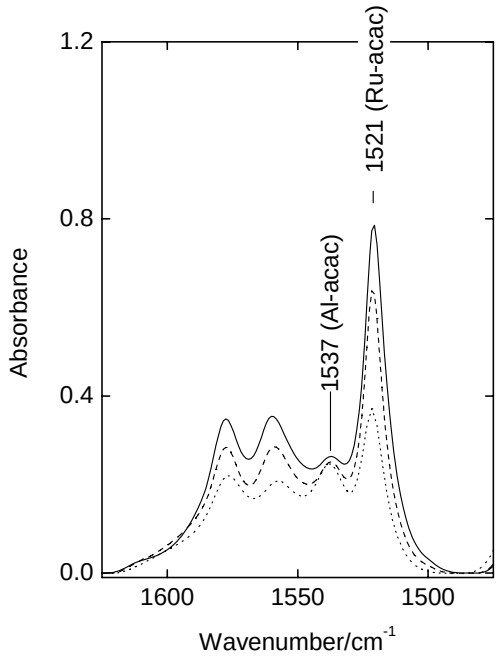

Figure 11S.

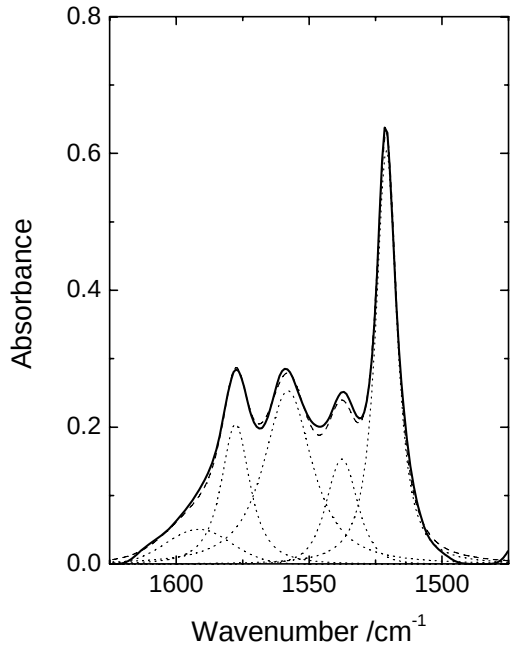

Figure 12S.

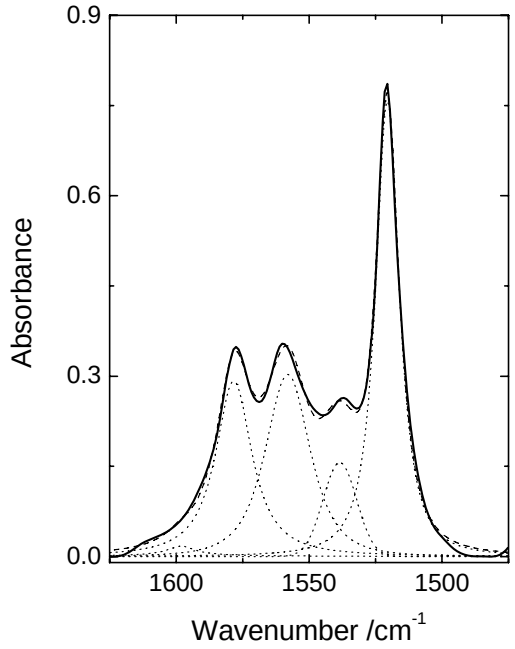

Figure 13S.

References

(1) Vaarkamp, M.; Linders, J. C.; Koningsberger, D. C. *Phys. B* **1995**, *209*, 159.

(2) Koningsberger, D. C.; Mojet, B. L.; van Dorssen, G. E.; Ramaker, D. E. *Top. Catal.* **2000**, *10*, 143.

(3) Zabinsky, S. I.; Rehr, J. J.; Ankudinov, A.; Albers, R. C.; Eller, M. J. *Phys. Rev. B* **1995**, *52*, 2995.

(4) Bennett, M. A.; Byrnes, M. J.; Willis, A. C. *Organometallics* **2003**, *22*, 1018.

(5) Pearson, W. B.; Calvert, L. D.; Villars, P. *Pearson's Handbook of Crystallographic Data for Intermetallic Phases*; American Society for Metals: Metals Park, OH, 1985.

(6) Error Reporting Recommendations: A Report of the Standards and Criteria Committee, Adopted by the International XAFS Society, Standards and Criteria Committee, July 26, 2000, Ako, Japan.
www.i-x-s.org/OLD/subcommittee_reports/sc/err-rep.pdf

(7) Kelly, S. D.; Kemmer, K. M.; Fryxell, G. E.; Liu, J.; Mattigod, S. V.; Ferris, K. F. *J. Phys. Chem. B* **2001**, *105*, 6337.

(8) Stern, E. A.; Newville, M.; Ravel, B.; Yacoby, Y.; Haskel, D. *Phys. B* **1995**, *209*, 117.